Send Orders for Reprints to reprints@benthamscience.net

Current Alzheimer Research, 2023, *20*, 440-452

RESEARCH ARTICLE

Towards the Integrative Theory of Alzheimer's Disease: Linking Molecular Mechanisms of Neurotoxicity, Beta-amyloid Biomarkers, and the Diagnosis[#]

Yaroslav I. Molkov[1], Maria V. Zaretskaia[2] and Dmitry V. Zaretsky[2,*]

[1]*Department of Mathematics and Statistics and Neuroscience Institute, Georgia State University, Atlanta, GA 30303, USA;* [2]*Zarbio, Chapel Hill, NC 27516, USA*

ARTICLE HISTORY

Received: December 27, 2022
Revised: June 16, 2023
Accepted: July 14, 2023

DOI:
10.2174/1567205020666230821141745

Abstract: ***Introduction*:** A major gap in amyloid-centric theories of Alzheimer's disease (AD) is that even though amyloid fibrils per se are not toxic *in vitro*, the diagnosis of AD clearly correlates with the density of beta-amyloid (Aβ) deposits. Based on our proposed amyloid degradation toxicity hypothesis, we developed a mathematical model explaining this discrepancy. It suggests that cytotoxicity depends on the cellular uptake of soluble Aβ rather than on the presence of amyloid aggregates. The dynamics of soluble beta-amyloid in the cerebrospinal fluid (CSF) and the density of Aβ deposits is described using a system of differential equations. In the model, cytotoxic damage is proportional to the cellular uptake of Aβ, while the probability of an AD diagnosis is defined by the Aβ cytotoxicity accumulated over the duration of the disease. After uptake, Aβ is concentrated intralysosomally, promoting the formation of fibrillation seeds inside cells. These seeds cannot be digested and are either accumulated intracellularly or exocytosed. Aβ starts aggregating on the extracellular seeds and, therefore, decreases in concentration in the interstitial fluid. The dependence of both Aβ toxicity and aggregation on the same process-cellular uptake of Aβ−explains the correlation between AD diagnosis and the density of amyloid aggregates in the brain.

***Methods*:** We tested the model using clinical data obtained from the Alzheimer's Disease Neuroimaging Initiative (ADNI), which included records of beta-amyloid concentration in the cerebrospinal fluid (CSF-Aβ42) and the density of beta-amyloid deposits measured using positron emission tomography (PET). The model predicts the probability of AD diagnosis as a function of CSF-Aβ42 and PET and fits the experimental data at the 95% confidence level.

***Results*:** Our study shows that existing clinical data allows for the inference of kinetic parameters describing beta-amyloid turnover and disease progression. Each combination of CSF-Aβ42 and PET values can be used to calculate the individual's cellular uptake rate, the effective disease duration, and the accumulated toxicity. We show that natural limitations on these parameters explain the characteristic distribution of the clinical dataset for these two biomarkers in the population.

***Conclusion*:** The resulting mathematical model interprets the positive correlation between the density of Aβ deposits and the probability of an AD diagnosis without assuming any cytotoxicity of the aggregated beta-amyloid. To the best of our knowledge, this model is the first to mechanistically explain the negative correlation between the concentration of Aβ42 in the CSF and the probability of an AD diagnosis. Finally, based on the amyloid degradation toxicity hypothesis and the insights provided by mathematical modeling, we propose new pathophysiology-relevant biomarkers to diagnose and predict AD.

Keywords: Alzheimer's disease, beta-amyloid toxicity, amyloid depositions, cellular uptake, lysosome.

*Address correspondence to this author at the Zarbio, Chapel Hill, NC 27516, USA; E-mail: dmitry.zaretsky@zar.bio

[#]*Data used in the preparation of this article were obtained from the Alzheimer's Disease Neuroimaging Initiative (ADNI) database (adni.loni.usc.edu). As such, the investigators within the ADNI contributed to the design and implementation of ADNI and/or provided data but did not participate in analysis or writing of this report. A complete listing of ADNI investigators can be found at: http://adni.loni.usc.edu/wp-content/uploads/how_to_apply/ADNI_Acknowledgement_List.pdf*

1. INTRODUCTION

Dr. Alzheimer first described extracellular senile plaques and intracellular neurofibrillary tangles as specific to a certain kind of dementia [1], later named Alzheimer's Disease (AD) [2]. The main component of the extracellular deposits is beta-amyloid protein (Aβ) [3, 4]. Aβ was found to be toxic to cultured cells [5-7]. Also, histopathological changes are more likely to occur in cells in close proximity to the plaques [8-10]. Based on this evidence, the etiology and pathogenesis of AD were associated by the scientific community with the Aβ plaques. Further, by means of the positron emission tomography (PET) technique, the density of amyloid deposits was measured in live subjects, which brought more indirect data supporting a potential role of Aβ in AD pathogenesis [11] as cognitively impaired AD patients had significantly denser amyloid deposits. Even more importantly, patients with a significant density of amyloid deposits appeared much more prone to decline cognitively in the future compared to amyloid-negative individuals [12].

The density of amyloid deposits negatively correlates with Aβ42 concentration in the cerebrospinal fluid (CSF) [13-15]. Due to the strength of this negative correlation, the overall diagnostic accuracy of CSF-Aβ42 and PET studies is considered similar [11]. However, CSF-Aβ42 levels and PET imaging data on the density of amyloid deposits were recently shown to have independent predictive powers for different Alzheimer's disease markers, including AD diagnosis itself, hippocampal volume, and brain metabolism [14]. Importantly, patients with AD tend to have lower CSF-Aβ42 levels than research subjects with normal cognition, even if their PET levels are the same [14, 16].

The decrease of CSF-Aβ42 with an increased density of amyloid deposits can be explained by a more intense aggregation of soluble amyloid on already aggregated amyloid. However, the aggregation cannot explain why decreased CSF-Aβ42 is associated with a higher probability of AD diagnosis at the same levels of amyloid load and hence the same aggregation rate. There are other factors that can affect the Aβ concentration in the CSF, such as the Aβ synthesis rate and the Aβ filtering rate, largely defined by the CSF flow intensity. Aβ synthesis is not lower in patients with AD [17], and the CSF flow is not more intense in patients with AD [18, 19]. Therefore, a decreased CSF-Aβ42 can only be explained by more intense clearance of the peptide inside the brain [20].

The most obvious mechanism of intratissue removal of Aβ42 is cellular uptake. The link between increased cellular uptake of beta-amyloid and increased neuronal death can be explained by the amyloid degradation toxicity hypothesis [21]. After endocytosis, beta-amyloid is digested by lysosomal proteases. Some peptide fragments can aggregate into oligomeric forms capable of creating membrane channels and thus permeabilizing lysosomal membranes which happen to have all the properties required to incorporate amyloid membrane channels [22, 23]. Lysosomal permeabilization is a well-established consequence of the exposure of cells to beta-amyloid [24, 25]. Amyloid channels can be extremely large [26-28], which would allow, according to our estimates, the release of lysosomal cathepsins into the cytoplasm [29]. Cytoplasmatic leakage of lysosomal proteases can activate necrotic and/or apoptotic processes [30-33], and thus be the molecular mechanism initiating neuronal death. However, the amyloid degradation toxicity hypothesis *per se* does not explain why the density of amyloid deposits correlates with the probability of AD diagnosis or has any prognostic value.

To better understand the nature of the correlation between the density of amyloid deposits, Aβ42 concentration in the CSF, and the progression of AD, we developed an integrative mathematical model describing beta-amyloid turnover and its connection to the diagnosis of AD. Based on the above, we assumed that cellular amyloid uptake is an important factor defining Aβ toxicity *in vivo*. The cognitive effect of Aβ toxicity accumulates over time, so cognitive decline is faster when cellular amyloid uptake is higher. The degree of neuronal damage induced by Aβ uptake varies between individuals due to either differences in the sensitivity to the toxic action of beta-amyloid or various mechanisms of protective response. Importantly, we hypothesized that due to the intensity of protein turnover, aggregation seeds do not form in the interstitial fluid but appear first intracellularly from the endocytosed Aβ. After being exocytosed, these seeds grow by aggregating soluble Aβ and become senile plaques. This hypothesis implicates cellular uptake as an underlying mechanism for both Aβ aggregation and cytotoxicity. In the present study, we used these assumptions to map the inferred beta-amyloid kinetics to the probability of AD diagnosis and compared the output of the model to the existing clinical dataset containing data on the Aβ concentration in the CSF and the density of amyloid deposits.

2. METHODS

2.1. Clinical Dataset

We used non-personalized data available through the Alzheimer's Disease Neuroimaging Initiative (ADNI) (http://adni.loni.usc.edu/). The ADNI was launched in 2003 as a public-private partnership led by Principal Investigator Michael W. Weiner, MD. The primary goal of ADNI has been to test whether serial magnetic resonance imaging, positron emission tomography (PET), other biological markers, and clinical and neuropsychological assessment can be combined to measure the progression of mild cognitive impairment (MCI) and Alzheimer's disease (AD). The study protocol for ADNI was approved by the local ethical committees of all participating institutions, and all participants signed informed consent, which included consent for de-identified data being shared with the general scientific community for research purposes [34]. The authors of this manuscript did not participate in data acquisition and received de-identified data after approval by ADNI.

Our analysis included all ADNI participants for whom the ascertainment of normal cognition (NC) or AD diagnosis, as well as CSF collection, were made within one year from a PET scan identifying brain amyloidosis. All subjects were evaluated between June 2010 and February 2019. Amyloid positivity was defined by PET data according to ADNI guidelines as a standard uptake value ratio (SUVR) at or above 1.08 for (18)F-florbetaben or 1.11 for (18)F-florbetapir, with a higher SUVR indicating a greater amyloid

plaque burden. Details regarding PET acquisition are described in previous publications and on the ADNI website (www.adni-info.org). Given the use of two different amyloid PET-tracers, SUVR levels were converted to centiloids (CL) using the specific equation for each tracer as provided by ADNI. Datapoints (the concentration of Aβ42 in the CSF *vs.* PET signal) included in this study are shown in Fig. (**1**).

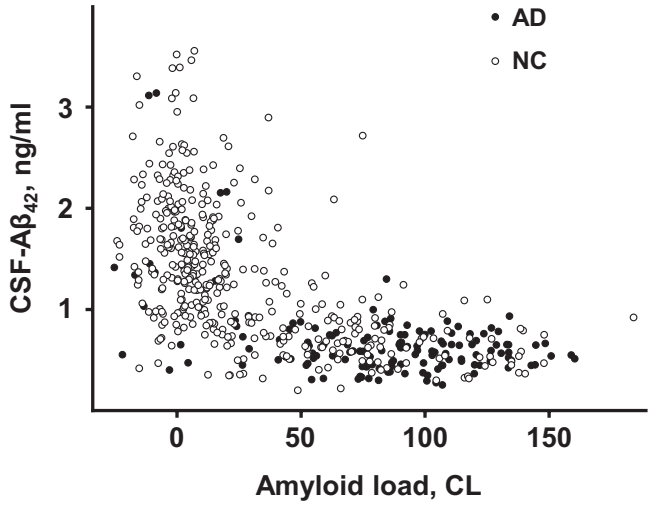

Fig. (1). ADNI data on CSF-Aβ42 *vs.* beta-amyloid load in research subjects with normal cognition (NC, open circles) and patients with Alzheimer's disease (AD, closed circles). *(A higher resolution / colour version of this figure is available in the electronic copy of the article).*

The characteristics of the two groups included in the study (AD *vs.* NC) are shown in Table **1**. Both groups have similar age distribution and number of years of education. NC group had an equal number of male and female subjects, while patients with AD had approximately 50% more males (61% of males *vs.* 39% of females). Average scores in the sum of boxes of the clinical dementia rating scale CDR (CDR-SB) and the Alzheimer's Disease Assessment Scale–Cognitive Subscale (ADAS-Cog-11) were higher, while the scores of Standardized Mini-Mental State Examination (MMSE) were lower in AD group compared to NC group. In line with general population data, the percentage of ApoE4 carriers was significantly higher in AD group, especially the percentage of carriers of two copies of ApoE4.

2.2. A Mathematical Model of the Cerebral Amyloid Turnover

The model employed in this study extends the ordinary differential equation (ODE) model we used previously [20]. The concentration of soluble Aβ in the interstitial fluid (ISF), denoted by [*ISF*], is controlled by several processes: (1) synthesis by cells, (2) filtration of the protein into the CSF, (3) aggregation into non-soluble plaques, and (4) uptake by cells (Fig. **2**). Beta-amyloid taken up by cells either is digested and initiates cytotoxicity or aggregates into fibrils which can be exocytosed. Cytotoxic insult is proportional to the amount of endocytosed CSF-Aβ42. In turn, exocytosed fibrils serve as seeds for beta-amyloid aggregation from the interstitial fluid. The rate of removal of soluble Aβ from the solution increases with the growth of these deposits.

The model and its analysis are based on the following assumptions:

1) Synthesis rate (SYN) is independent of both interstitial Aβ42 and the density of plaques.
2) The rate of removal of protein through the CSF is a product of the CSF flow ($FLOW_{CSF}$) and CSF-Aβ42 ($[CSF]$): $FLOW_{CSF} \cdot [CSF]$.
3) The model assumes a linear relationship between the concentrations of soluble Aβ42 in the ISF and the CSF with a coefficient of transfer K_T: $[CSF] = K_T \cdot [ISF]$.
4) The rate of cellular uptake of soluble Aβ42 ($Uptake$) is proportional to the interstitial Aβ42 concentration $[ISF]$ with a coefficient of uptake K_u: $K_u \cdot [ISF]$.
5) The exocytosis of intracellularly produced fibrils is proportional to the $Uptake$, and therefore is proportional to $[ISF]$: $K_{exc} \cdot Uptake = K_{exc} \cdot K_u \cdot [ISF]$.
6) Existing plaques serve as seeds for the aggregation of soluble Aβ42 in the ISF. The rate of loss of soluble Aβ42 from the ISF due to aggregation is a product of Aβ42 concentration in the ISF, the concentration of plaques ($[PET]$, calculated from the intensity of the PET signal), and the coefficient of aggregation K_a: $K_a \cdot [PET] \cdot [ISF]$.
7) Current intensity of toxic insult (current toxicity) is proportional to the uptake: $K_{tox} \cdot Uptake$.
8) Neural damage (accumulated toxicity, TOX) is an integral of current toxicity over the duration of illness (T_{ill}).

Under these assumptions, the system of ordinary differential equations describing the dynamics of beta-amyloid concentrations in the ISF and CSF, and the density of amyloid deposits characterized by the PET signal will have the following form:

$$\frac{d}{dt}[ISF] = SYN - K_u \cdot [ISF] - K_a \cdot [PET] \cdot [ISF] - Flow_{CSF} \cdot [CSF], \quad (1)$$

$$\frac{d}{dt}[PET] = K_{exc} \cdot K_u \cdot [ISF] + K_a \cdot [PET] \cdot [ISF], \quad (2)$$

where $[CSF] = K_T \cdot [ISF]$, with an initial condition $[PET] = 0$ at $t = 0$. Assuming that the time scale of soluble Aβ42 dynamics is much shorter than the time scale of beta-amyloid deposits accumulation, so at each time Aβ42 concentration in ISF/CSF is at instantaneous equilibrium, one can show that $[CSF]$ and $[PET]$ satisfy the following relationship:

$$K_u = K_a \cdot \left(\frac{S}{[CSF]} - F - [PET]\right), \quad (3)$$

where F and S are compound parameters proportional to $Flow_{CSF}$ and SYN, respectively: $F = K_T/Ka \cdot Flow_{CSF}$; $S = K_T/Ka \cdot SYN$. Using the above relationship, Eq. (2) can be solved, and explicit expressions for the accumulated toxicity and the disease duration can be obtained:

$$TOX = \int_0^{T_{ill}} K_u \cdot [ISF]dt = \frac{K_u}{K_a} ln\left(1 + \frac{K_a \cdot [PET]}{K_{exc} \cdot K_u}\right); \quad (4)$$

$$T_{ill} \cdot SYN = [PET] + (K_u \cdot (1 - K_{exc}) + F)\, ln\left(1 + \frac{K_a \cdot [PET]}{K_{exc} \cdot K_u}\right) \quad (5)$$

Note, Eqs. (3) and (4) together allow calculating the accumulated toxicity for an individual based on their current

Table 1. Basic characteristics across cognitive categories in the research population. The means and standard deviations are specified for continuous variables. For discrete variables, the percentage of subjects with the given parameter value is shown.

Variable	AD (N=143)	NC (N=476)
Age (years)	74.6 (8.2)	73.8 (6.0)
Education (years)	15.7 (2.7)	16.6 (2.6)
CDR-SB	4.7 (1.9)	0.3 (1.1)
ADAS-Cog-11	20.7 (7.0)	6.2 (4.3)
MMSE	22.8 (2.5)	28.7 (1.9)
Males (%)	61	50
ApoE4, 0 copies (%)	31	74
ApoE4, 1 copy (%)	47	24
ApoE4, 2 copies (%)	22	2

Abbreviations: AD, Alzheimer's disease; NC, normal cognition; CDR-SB, sum of boxes of the clinical dementia rating; ADAS-Cog-11, Alzheimer's Disease Assessment Scale–Cognitive Subscale; MMSE, Mini-Mental State Examination; ApoE4, E4 version of the apolipoprotein E gene.

readings of the CSF-Aβ42 and Aβ deposit density (the intensity of PET signal).

2.3. Mapping the Accumulated Toxicity to the Probability of AD Diagnosis

We assume that each individual has their own toxicity threshold T, so they become sick with AD if their accumulated toxicity exceeds this threshold. We further assume that the probability distribution of the toxicity thresholds in the population is normal with a certain mean T_0 and variance σ_T^2. Therefore, the probability of AD based on the individual's accumulated toxicity can be calculated using the cumulative distribution function (CDF) of the normal distribution as follows.

$$p = Prob\{TOX > T\} = \frac{1}{2}\left[1 + \mathrm{erf}\left(\frac{TOX - T_0}{\sigma_T\sqrt{2}}\right)\right] \quad (6)$$

where erf(.) is the error function.

2.4. Parameter Inference

In terms of the number of participants, the ADNI dataset we used is biased towards patients with AD diagnosis (~26%) compared to 10% of similar age patients in the general population [35]. To account for this discrepancy, we created a surrogate dataset by triplicating records of the healthy participants. This resulted in the corrected fraction of AD patients in the group reflecting the one observed in the general population.

For each participant, the AD diagnosis X is a Boolean random variable having the Bernoulli distribution (a particular case of the binomial distribution $B(1, p)$) with the above probability, which is a function of Aβ42 concentration in CSF, the PET signal as well as 5 unknown parameters, T_0, σ_T, $Kexc$, S and F. AD diagnoses of different participants are assumed independent. Therefore, the likelihood function for the ADNI dataset is as follows:

$$L(T_0, \sigma_T, Kexc, S, F) = \prod_{i=1}^{N} p_i^{X_i}(1 - p_i)^{1-X_i} \quad (7)$$

where N is the total number of datapoints, $X_i = 1$ if the i^{th} participant is diagnosed with AD, $X_i = 0$ otherwise, and $p_i = p([PET]_i, [CSF]_i; T_0, \sigma_T, Kexc, S, F)$ is the probability of AD diagnosis given the measured values $[PET]_i$ and $[CSF]_i$ of the i^{th} participant as defined by Eq. (6). To identify the parameter values, we used the Maximum Likelihood Estimation (MLE) method. Specifically, by the gradient descent method, we found the values of the 5 model parameters corresponding to the maximum of the likelihood function (7). Hereinafter we refer to those as the MLE parameter values. In this procedure, datapoints which either had negative PET values or resulted in negative values of the uptake rate were assumed outliers and were excluded from the consideration.

2.5. Model's Goodness-of-fit Evaluation

To evaluate how well the model output corresponds to the ADNI data, we used Pearson's chi-square test. We partitioned the (PET, CSF)-plane into non-overlapping rectangular cells with dimensions of 25 CL by 500 pg/ml. We calculated the number of AD patients (x_i) and cognitively normal participants in each cell. These numbers were corrected by the factors of 0.4 and 1.2, respectively, to adjust the fraction of AD patients to 10% (see above), while keeping the overall number of participants the same (see the supplemental spreadsheet for calculations). We used Eq. (6) to calculate the expected number of AD patients in the center of each cell as a product of the total number of participants in this cell (n_i) and the probability of AD diagnosis (p_i), as predicted by the model with MLE parameter values. Then we constructed a chi-square statistic as follows:

$$\chi^2 = \sum_{i=1}^{k} \frac{(x_i - n_i p_i)^2}{n_i p_i (1 - p_i)},$$

where $k = 23$ is the number of cells with non-zero number of participants. If the model fits well, the calculated statistic

should be a sample from a chi-square distribution. The number of degrees of freedom of the chi-square distribution equals the number of cells used (23 cells) minus the number of model parameters subject to optimization (5 parameters). Using this distribution, we calculated the p-value as the probability of the chi-square statistic to exceed the calculated value. We accepted 0.05 as the significance level.

3. RESULTS

3.1. The Model Accurately Predicts the Fraction of AD Patients based on the Values of PET and CSF-Aβ42

We found the following values of the model parameters using the Maximum Likelihood Estimation approach (see Methods): $S = 250$ CL·ng/ml, $F = 78$ CL, $K_{exc} = 0.47$, $T_0 = 190$ CL, and $\sigma_T = 87$ CL.

Fig. (**3A**) shows the probability of an AD diagnosis, calculated using these parameter values, as a function of CSF-Aβ42 and amyloid load (PET). The region of possible PET and CSF-Aβ42 values has an upper boundary representing a zero-uptake rate ($K_u = 0$), i. e. $S/CSF - F - PET = 0$. Experimental data are superimposed onto the theoretical probability distribution with measurements obtained from participants with normal cognition shown in green and measurements obtained from AD patients shown in yellow. Several experimental points that appear above the theoretical upper boundary are marked as outliers and removed from consideration. Goodness-of-fit of the model was evaluated using Pearson's chi-square test ($p = 0.19$, see Methods, Supplemental Materials). We conclude that the model prediction of AD diagnosis based on the PET and CSF-Aβ42 readings fits the experimental data at a 95% confidence level.

3.2. Positive Correlation between the AD Diagnosis and the Density of Amyloid Deposits

The proposed model readily explains the positive correlation between an AD diagnosis and the density of amyloid deposits without a causal effect of amyloid deposits on neurotoxicity. Indeed, if CSF-Aβ42 levels are not considered, the probability of AD diagnosis, as calculated by the model, increases with amyloid load (Fig. **3B**).

The total amyloid uptake can be represented as a product of the time-averaged cellular uptake rate and the duration of disease. Since our model allows for estimating the latter (see Eq. (3) in Methods), we analyzed curves representing the hypothetical AD "age" of participants (Fig. **3B**) calculated based on their current PET and CSF-Aβ42 readings. Unsurprisingly, longer disease durations generally correspond to greater accumulated amyloid deposits. However, this accumulation depends on CSF-Aβ42 in a non-trivial way (see Eq. (2) in Methods. Specifically, for long-enough disease durations (see curve 3.5 in Fig. **4B**), the accumulated deposits are maximal at intermediate CSF-Aβ42 values (0.5-1 ng/ml). In general, CSF-Aβ42 negatively correlates with the cellular amyloid uptake rate (see more on that below), so an increase in CSF-Aβ42 corresponds to an effective decrease in cellular amyloid uptake, and, therefore, a slower excretion of amyloid seeds (see Fig. **2**). On the other hand, extremely low CSF-Aβ42 levels lead to a reduction in amyloid aggregation on already excreted seeds and somewhat lower PET levels for the same disease duration (see the lower part of the curve 3.5 in Fig. **4B**).

3.3. Negative Correlation between CSF-Aβ42 and AD Diagnosis

Another important clinical observation that can be explained by the model is that, at the given density of amyloid deposits, the probability of AD diagnosis increases as CSF-Aβ42 reduces (Fig. **3C**). According to the model, at the highest possible levels of CSF-Aβ42, the probability of AD diagnosis is low due to a small cellular uptake rate. An increase in amyloid removal through uptake leads to lower CSF-Aβ42, as well as to elevated neurotoxicity. Again, our model assumes that lower CSF-Aβ42 levels *per se* are not causal to more intensive neurodegeneration. Rather, both processes result from increased cellular uptake.

Level curves corresponding to several different uptake rate values (see Eq. (1) in Methods) are shown in Fig. (**4A**). At the uppermost curve labeled "K_u = 0" the uptake rate equals 0, and all data points appearing above this curve are considered outliers (see Methods) since, according to the model, values of CSF-Aβ42 above this curve would correspond to negative values of the uptake rate. As we increase the amyloid uptake rate, the corresponding level curves occur progressively lower, reflecting a reduction in CSF-Aβ42 caused by higher uptake. At the same time, the probability of AD diagnosis increases (Figs. **3A, C**) due to the increased cellular uptake of amyloid. This explains why the average uptake rate in the AD group appears higher than in the participants with normal cognition [20] (Fig. **4A**). We illustrated this phenomenon by showing the level curves corresponding to the uptake rate averages for cognitively normal participants and AD patients (K_u = 1.5 and K_u = 2.9, respectively, in Fig. **4A**). At extremely high uptake values, the level curves become nearly horizontal and serve as a lower boundary for CSF-Aβ42 (see K_u = 8 in Fig. **4A**).

3.4. The Model Explains the Shape of the Dataset on the (PET, CSF-Aβ42)-plane

The distribution of data points on the (PET, CSF-Aβ42)-plane has a characteristic shape (Figs. **1** and **4**). Natural limitations on the parameters of the model can serve as the boundaries of this cloud (Fig. **4D**). As noted, the upper boundary results from the fact that the cellular uptake rate cannot be negative. Therefore, physiologically plausible values of CSF-Aβ42 must satisfy the inequality

$$CSF < \frac{S}{F + PET}$$

which follows from Eq. (1) in Methods (see K_u = 0 in Fig. **4A**).

The lower boundary in terms of CSF-Aβ42 appears horizontal, *i.e.*, the lowest possible values of CSF-Aβ42 are almost independent of the density of amyloid deposits characterized by PET. This lower boundary corresponds to highest possible uptake rate values that make intratissue clearance much greater than the aggregation (see K_u = 8 in Fig. **4A**). Highest uptake corresponds to an approximate minimal pos-

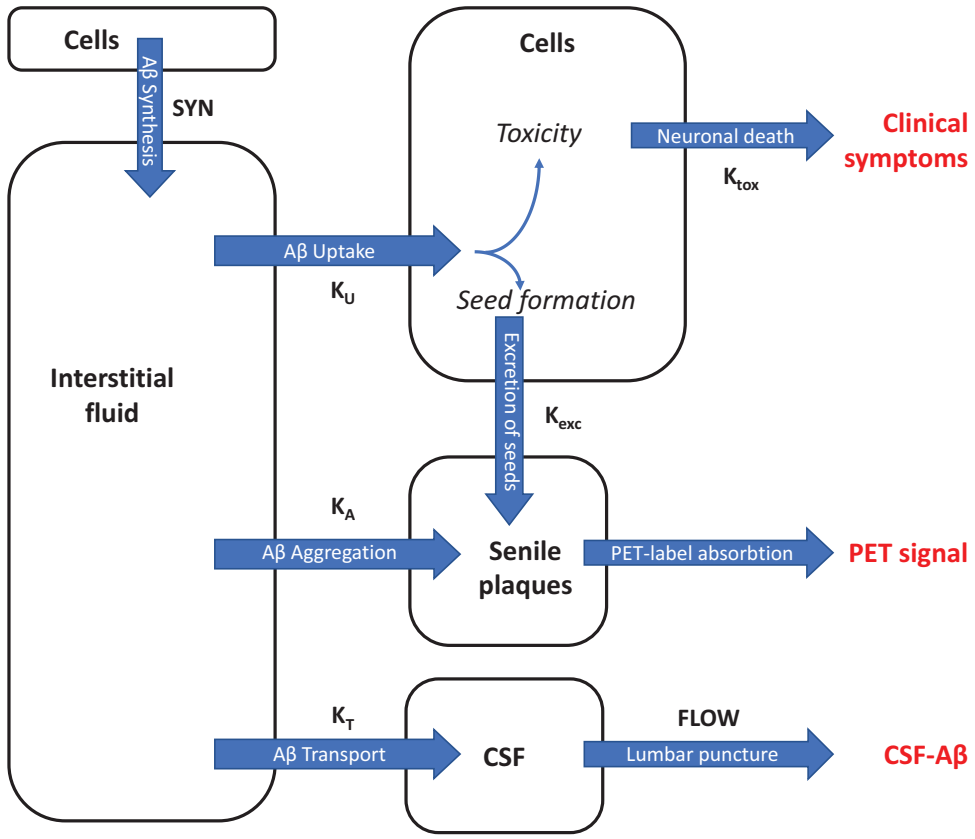

Fig. (2). Schematic of the model of beta-amyloid turnover describing the mathematical relationship between Aβ cytotoxicity, which leads to Alzheimer's disease (AD), and two biomarkers of AD: CSF-Aβ42 (measured in the CSF collected by lumbar puncture) and amyloid load in the brain (measured using positron-emission tomography). The parameters of the model are shown next to the arrows. *(A higher resolution / colour version of this figure is available in the electronic copy of the article).*

sible CSF-Aβ42 value of 0.3 ng/ml (which is approximately equal to $S/8$).

On the right, the cloud is bounded by the maximum possible PET values, which correspond to the largest possible density of amyloid deposits. Accumulation of the aggregated amyloid is limited by the disease's lifespan. Therefore, the right boundary can be described by the level curve of the disease duration corresponding to the participants with the longest times of disease progression. Note that the curve corresponding to the longest disease progression also serves as an upper boundary (compare curves $T_{ill} = 3.4$ and $K_u = 0$ in Fig. **4D**).

Finally, it is reasonable to expect that very high accumulated toxicity levels should be incompatible with survival, and, therefore, we would not see participants corresponding to those levels. Fig. (**4C**) shows the level curves for accumulated toxicity/AD diagnosis probability. One can observe that indeed, the curve corresponding to an AD diagnosis probability of 0.7 fits well as the lower boundary of the cloud around 150 CL PET values (see curve $p = 0.7$ in Fig. **4C**).

4. DISCUSSION

Recent history of scientific progress in Alzheimer's disease research is filled with controversies regarding the role of the most prominent and well-known anatomical correlate of the disease, the amyloid plaques. Even though the density of the plaques has a strong correlation with the clinical status of the patient, not all patients with a high amyloid load have the disease [36]. Also, the Aβ concentration used in cell cultures for the toxicity studies exceeds the naturally observed one by several orders of magnitude (ng/ml in the CSF [15, 16, 37] *vs.* μg/ml in *in vitro* toxicity experiments [5, 7, 38]). The lack of/minimal effectiveness of the drugs targeting Aβ in clinical trials [39-41] further undermines the confidence that beta-amyloid deposits are in fact relevant to AD etiology and pathogenesis.

Nevertheless, the correlations between the presence of Aβ aggregates in the brain, the concentration of Aβ42 in the CSF, and the clinical status of the patients are obvious and beg for some mechanistic explanations. Considering that Aβ is, in fact, toxic to cells [5-7], we have built a mathematical model connecting molecular mechanisms of amyloid toxicity to clinical data contained in the ADNI database available to researchers through an extensive public-private partnership [42, 43]. Here, we discuss the basis of our model's assumptions and how it resolves the controversies.

4.1. Main Assumptions of the Model

4.1.1. Mechanism of Beta-amyloid Toxicity

The cytotoxic effect of Aβ in the model is based on the amyloid degradation toxicity hypothesis [21]. This hypothesis has the following cornerstones.

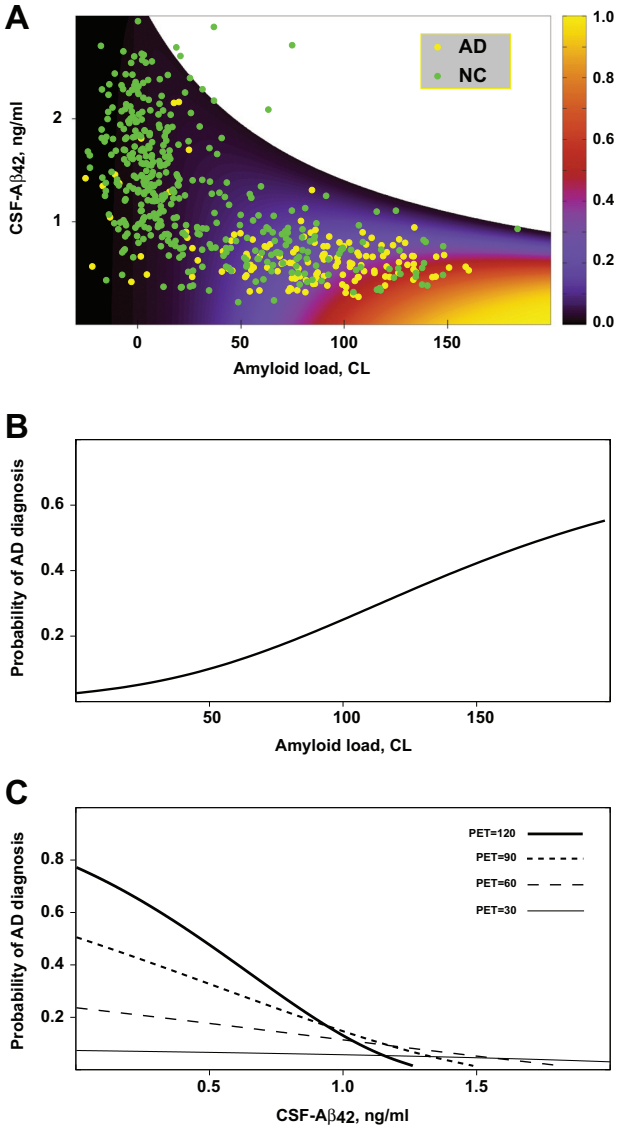

Fig. (3). The model tuned to clinical data. (**A**) The probability of Alzheimer's disease as a function of CSF-Aβ42 and amyloid load based on the best-fit parameters of the model. The overlain scatter plot shows data points indicating subjects with normal cognition (NC, green circles) and patients with Alzheimer's disease (AD, yellow circles). (**B**) Probability of AD diagnosis as a function of beta-amyloid load calculated using the model under the assumption that, for any given amyloid load, the values of CSF-Aβ42 are uniformly distributed in the range corresponding to the experimentally measured values. (**C**) Probability of AD diagnosis as a function of CSF-Aβ42 for various levels of amyloid load. *(A higher resolution / colour version of this figure is available in the electronic copy of the article).*

First, the molecular mechanism of Aβ toxicity is the permeabilization of cellular membranes by membrane channels formed by amyloid oligomers. This is similar to the membrane channel hypothesis first introduced in the early 1990s by Arispe *et al.* [26, 44-46].

Second, we assume that channels are formed by Aβ degradation products. We previously demonstrated that the 42 amino acids-long Aβ peptide does not effectively form membrane channels, while the undecapeptide Aβ25-35 does [22, 23]. The latter is one of the products of the proteolytic degradation of the full-length peptide, also known for its extreme neurotoxicity [47]. So, unlike the original amyloid membrane channel hypothesis, we assume that the fragments (such as Aβ25-35), rather than the full-length peptide, are largely responsible for the formation of the channels. It is possible that membrane channels can be formed by various fragments [28, 48, 49].

Third, the channels occur in the lysosomal membranes, rather than in the plasma membrane. Due to a positive charge of the Aβ25-35, these fragments can form channels in the negatively charged membranes only [22, 23, 50]. The outer leaflet of plasma membrane is mostly neutral in healthy cells [51]; however, some intracellular membranes, such as the inner mitochondrial and lysosomal membranes, have a significant negative surface charge [21, 22]. While the delivery route to the inner mitochondrial membranes is unclear, the lysosomal membranes are obvious targets for Aβ-induced damage. Indeed, Aβ was previously shown to be endocytosed and found intralysosomally [24, 25, 52]. Next, lysosomes contain various proteases and are responsible for peptide degradation with Aβ25-35 being one of the products [47]. It is quite possible that some other Aβ fragments can also form membrane channels [48].

These three basic assumptions can qualitatively explain several important features of AD, such as lysosomal dysfunction, mitochondrial damage, increased apoptosis, *etc.* [53-58]. They also imply that the neurodegeneration rate depends on the intensity of the lysosomal permeabilization process, which is in turn defined by the Aβ influx through endocytosis. In line with that, in the model, the toxic effect of Aβ is proportional to the amount of endocytosed peptide (Fig. **2**). Throughout the manuscript, we refer to this process as cellular amyloid uptake.

4.1.2. Formation of Amyloid Deposits

Aβ is synthesized in the form of propeptide that undergoes proteolytic processing and is released into the interstitial fluid [59]. In terms of concentration, a major form of beta-amyloid is Aβ40 (40 amino acids-long peptide). However, unlike Aβ40, the second most prominent form, Aβ42 (42 amino acids-long peptide), has a strong correlation with AD diagnosis [60, 61]. Aβ42 is also more prone to aggregation through the formation of beta-sheets [61].

The process of Aβ aggregation is non-linear. Aβ is synthesized and released into the interstitial fluid without any specific conformation. To initiate the aggregation process, it is necessary to create aggregation seeds first, which grow quickly after that. In experimental conditions, at the concentration of peptide in a μM range, the seeding of Aβ42 takes many hours [62, 63]. By extrapolating to the interstitial concentration of beta-amyloid *in vivo*, which is in an nM range, the seeding would take several months [63]. This makes spontaneous seeding in the interstitial space negligible over the typical time interval between the appearance of the monomeric molecule in the ISF and its clearance from the ISF through any mechanism: the half-life of brain Aβ42 is measured in hours [64]. However, after endocytosis, the intralyso-

somal concentration of amyloid is almost 100 times higher than its extracellular concentration [52, 65]. In lysosomes, the peptide remains enclosed intravesicularly for more than 24 hours [52, 66], thus providing the proper conditions and time needed for seed formation. The resistance of aggregated Aβ42 to proteolysis explains its intracellular accumulation [65]. Non-digestible inclusions are exocytosed; in the case of amyloid aggregates, they serve as aggregation seeds in the extracellular space attracting and appending the soluble Aβ [67].

Thus, in the model, the rate of change of the amyloid deposit density has two terms (see Eq. (2) in Methods, Fig. **2**). The first one represents the intracellular formation of amyloid fibrils, whose intensity is proportional to the cellular amyloid uptake. The second term represents the aggregation process on the already-formed deposits, with a rate proportional to the product of the interstitial Aβ42 concentration and the current amyloid deposit density.

4.1.3. Translating Neurotoxicity into AD Diagnosis

As noted, in the model, the intensity of the toxic insult is proportional to the rate of amyloid uptake by neurons, and the ultimate neuronal damage accumulates over time. However, the total amount of Aβ consumed by neurons may not define the degree of neuronal death by itself due to individual differences in sensitivity (resistivity) to its toxicity for the following reasons. First, the concentration of the toxic amyloid forms may depend on the balance between their creation and degradation. The fragmentation of the full-length peptide is mediated by exoproteases, while further degradation of fragments is performed by endoproteases. These processes may be mediated by different enzymes (even though some lysosomal proteases have both endo- and exo-proteolytic activity). The balance of these two proteolytic activities may have individual-to-individual variability. Also, any biochemical damage caused may be offset by protective and/or reparatory processes. For example, the damage from leaking cathepsins can be prevented by cytoplasmic protease inhibitors, such as cystatins [68]. Most likely, there are many other factors affecting the relationship between the intensity of Aβ uptake and neurotoxicity.

To account for these individual factors in the model, the development of the disease is considered probabilistic. Specifically, the overall toxic effect is proportional to the amyloid uptake accumulated over time (see Eq. (4) in Methods). The individual threshold for the accumulated toxicity leading to an AD diagnosis is assumed to be randomly distributed over the population. This way, the probability for a participant with a given accumulated toxicity to have an AD is numerically equal to the cumulative distribution function of the distribution of the thresholds (see Eq. (6) in Methods).

4.2. The Model Explains Previously Paradoxical Clinical Observations Related to the Density of Amyloid Deposits and Aβ42 Concentration in the CSF

As noted, one of the greatest controversies in the field is that the occurrence of Alzheimer's disease and its progression strongly correlates with the accumulation of extracellular amyloid deposits [11, 12], despite the aggregated Aβ is not toxic *in vitro* by itself [5, 7]. Our model accurately reproduces this correlation (Figs. **3A** and **B**) without any underlying assumptions about the neurotoxicity of the amyloid deposits. In the model, both amyloid aggregation and its toxicity depend on the internalization of soluble Aβ. Therefore, an increase in the cellular amyloid uptake intensifies the accumulation of both amyloid deposits and its neurotoxic effects (Fig. **2**). Both elevated neurodegeneration and higher accumulation of amyloid plaques in AD originates from increased cellular amyloid uptake. The fact that neuronal death and the accumulation of amyloid plaques have the same origin manifests as a positive correlation between the probability of AD diagnosis and amyloid load (Fig. **3B**).

Another strikingly paradoxical observation is that Alzheimer's disease and its progression are associated with the decreased concentration of soluble Aβ42 in the cerebrospinal fluid [13-15], despite, unlike aggregated Aβ, soluble Aβ forms are cytotoxic *in vitro* [5-7]. Due to aggregation of soluble Aβ42 on the exocytosed seeds and existing plaques, the concentration of soluble Aβ42 in the interstitial liquid becomes lower at higher amyloid load levels. Considering that the density of plaques positively correlates with the probability of AD diagnosis, it is not too surprising that CSF-Aβ42 levels are lower in AD patients. However, CSF-Aβ42 is lower in AD patients compared to subjects with normal cognition, even if they have the same amyloid load [14, 16]. This seems counterintuitive, as lower CSF-Aβ42 implies lesser Aβ42 availability for endocytosis. However, our model reproduces a negative correlation between CSF-Aβ42 and AD probability at a fixed amyloid load too (Fig. **3C**). The reason for this phenomenon is that lower CSF-Aβ42 levels are in this case caused by higher cellular amyloid uptake rates, resulting in an overall greater amount of amyloid being endocytosed and, therefore, its increased neurotoxicity.

4.3. The Model Describes the Distribution of PET and CSF-Aβ42

The distribution of clinical data in coordinates (PET, CSF-Aβ42) is not uniform (Fig. **1**). Specifically, CSF-Aβ42 has a wide range of values at low levels of PET. With increased PET, the CSF-Aβ42 range becomes progressively smaller due to decreasing maximal CSF-Aβ42 values, whereas the lower CSF-Aβ42 boundary remains relatively constant. Our analysis of the model shows that the upper and lower boundaries of this data cloud match the curves corresponding to a zero and a largest possible value of the cellular amyloid uptake rate, respectively (Fig. **4A**). The zero-uptake curve has a hyperbolic shape reflecting a reduction in the maximal physiologically possible values of CSF-Aβ42 with an increasing amyloid load, while the maximum uptake line (dashed line in Fig. **4A**) is almost horizontal.

The right boundary of the cloud in (Fig. **1**), corresponding to the maximal PET values, fits well with the longest disease progression time. We considered a family of isochrones on the (PET, CSF-Aβ42)-plane corresponding to progressively longer sickness (Fig. **4B**) and noticed that one of them can serve as the right boundary of the cloud (Fig. **4C**). Based on this, we can speculate that the right boundary corresponds to the longest times of the disease's progression, which may correlate with the maximal age of the participants. Note, however, that we do not make any assumptions

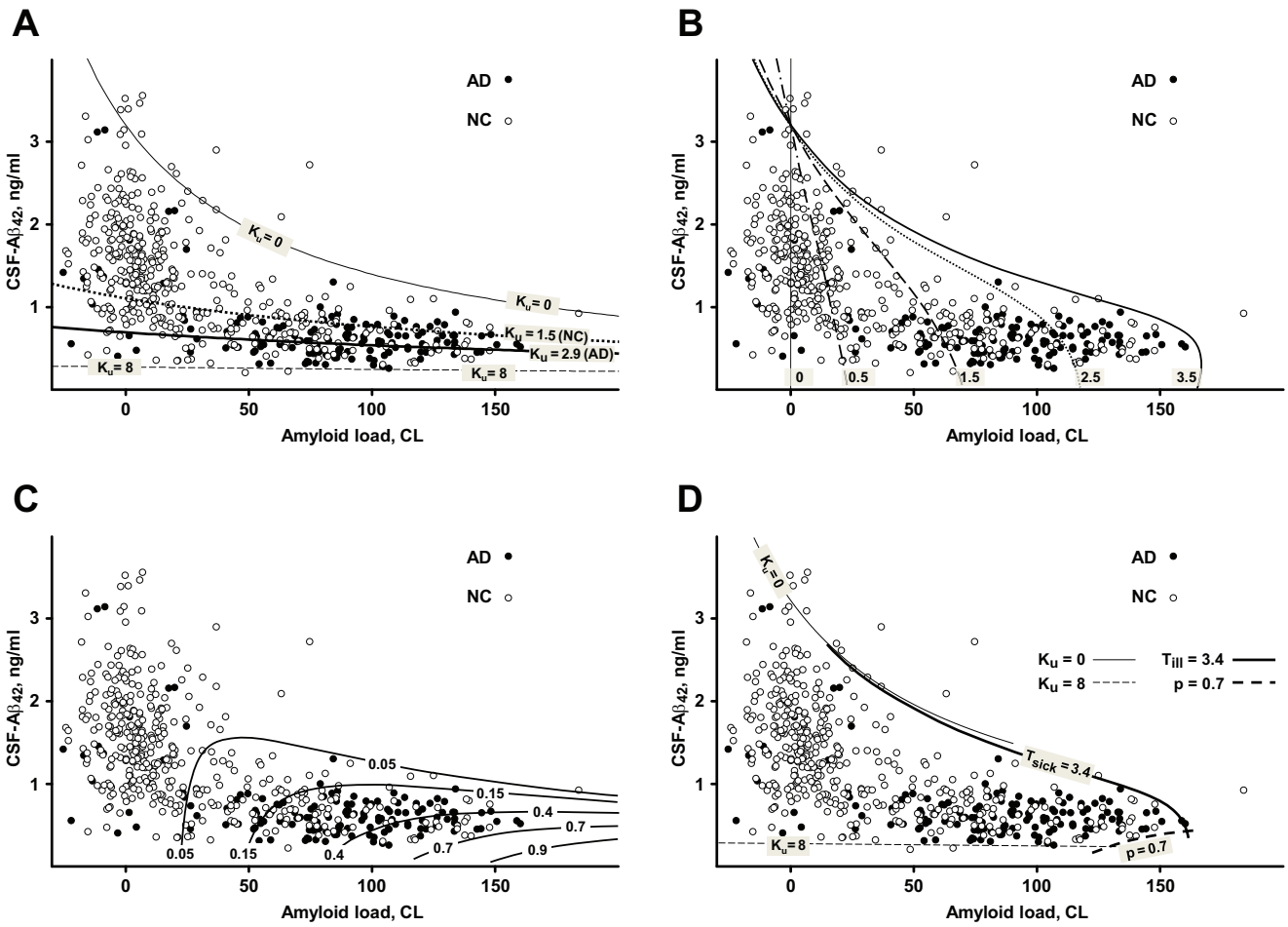

Fig. (4). Level curves for various values of the cellular uptake rate, the disease duration and the diagnosis probability in relation to the distribution of clinical data points. The uptake rate and the disease duration are in arbitrary units. The distributions of datapoints from research subjects with normal cognition (NC, open circles) and patients with Alzheimer's disease (AD, closed circles) are shown as the scatter plot of CSF-Aβ42 (ng/ml) *vs.* beta-amyloid load (centiloids, CL). (**A**) Level curves for the uptake rate are ordered from top to the bottom with an increasing value of the uptake rate. The curves corresponding to the average uptake rates for NC subjects and AD patients are shown as dotted and thick solid lines, respectively. (**B**) Level curves of the disease duration indicated by the labels next to the curves. (**C**) Level curves of the probability of AD diagnosis labelled by the corresponding probability values. They also represent the accumulated toxicity level curves with the corresponding accumulated toxicity values. (**D**) The cloud of datapoints in the clinical dataset is bounded by (1) minimal and maximal cellular uptake rate values (solid and dashed thin lines, correspondingly); 2) the maximal disease duration (thick solid line labeled T_{ill}= 3.4); (3) highest accumulated toxicity (thick dashed line; the probability of AD diagnosis p = 0.7). *(A higher resolution / colour version of this figure is available in the electronic copy of the article).*

in the model about the link between the length of the disease and the biological age.

The shape of the distribution of amyloid biomarkers in the ADNI dataset is similar to reported elsewhere [36]. However, there are no other known to us datasets of amyloid biomarkers, which have sufficient size and validated measurement protocol, which would allow for the testing of the model using independently collected data.

4.4. The Model Suggests New AD Biomarkers

In this study, we developed a theoretical basis for correlations between AD diagnosis probability and two extensively used AD biomarkers, Aβ42 concentration in the CSF and the density of amyloid deposits characterized by PET. Using the model, we identified two independent factors defining this probability that are the individual rate of the cellular amyloid uptake and disease duration.

The disease duration is not equivalent to the patient's biological age as the amyloid accumulation is known to start in middle age [69]. In the model, we can interpret the initiation of the disease as a stepwise increase in the cellular amyloid uptake rate at some point in life, which jumpstarts the disease progression. Therefore, monitoring and/or controlling this parameter may be instrumental in AD screening/managing at very early stages.

While there are no ready-to-use techniques to measure the cellular amyloid uptake, the stable isotope labeling kinetic (SILK) technique could be a good starting point [70], even though it is labor intensive and invasive. Interestingly, two parameters inferred using the SILK technique (v_{42} and k_{ex42})

that are likely to be associated with the cellular uptake of Aβ42 are, in fact, increased severalfold in patients with early-onset AD [70].

It is clear that higher CSF-Aβ42 correlates with a milder disease status, and probably, with a better prognosis, and is likely to contain information independent on the density of amyloid deposits [14]. However, until now, there was no mechanistic approach to using both biomarkers, CSF-Aβ42 and PET. According to our model, CSF-Aβ42 is lowered by higher cellular uptake, and data points for the patients with the lowest uptake rates (and corresponding to better disease status and prognosis) are located along the upper edge of the distribution. More generally, with limitations described above, the model allows estimating the rate of cellular amyloid uptake in a particular patient using the concentration of Aβ42 in the CSF and the density of amyloid deposits measured by PET.

In the model, we describe the AD diagnosis probabilistically, meaning that the same accumulated toxicity may or may not result in AD in a given individual. This implies that people have different toxicity thresholds quite broadly distributed over the population. Therefore, AD prevention can be based on heightening the amyloid toxicity thresholds. For example, per the amyloid degradation toxicity hypothesis, cytotoxicity occurs when specific amyloid fragments form membrane channels in the lysosomal membranes [21]. Correspondingly, the balance of endo-/exoproteolytic activities promoting or preventing the formation of channel-forming fragments could be a predictor of AD progression rate. These channels allow for the leakage of lysosomal cathepsins, which in turn activates the cell's necrosis or apoptosis. So, one of the ways to fight these toxic effects is to neutralize leaked cathepsins using some protease inhibitors such as cystatins [71].

Clearly, exploiting any of these routes requires new extensive studies focused on amyloid endocytosis and the mechanisms of amyloid cytotoxicity.

CONCLUSION

Since AD was associated with amyloid plaques, amyloid deposits have been pharmacological targets in hopes that their dissolvement can slow down disease progression. Our model offers a new perspective on this intensely debated topic. Considering that amyloid deposits are not toxic in the model, their disappearance will not have any consequences by itself. However, a decrease in the aggregated amyloid concentration will reduce the aggregation rate of soluble amyloid and thus increase its concentration in the ISF and CSF. The general relationship between CSF-Aβ42 and the density of amyloid deposits is provided by Eq. (3). According to this equation, dissolving the existing deposits should increase CSF-Aβ42, which is in fact observed clinically after dissolving senile plaques after the treatment with monoclonal anti-amyloid antibodies [39]. Our model's prediction is that the dissolvement of the amyloid plaques can only accelerate AD progression. From this perspective, not only is dissolving plaques not helpful but potentially harmful, and a high density of amyloid plaques appears protective rather than dangerous.

Our model does not consider the plaques toxic by themselves, which is not necessarily the case. For example, it was previously suggested that amyloid deposits could activate inflammatory responses or be the source of oxidative stress due to absorbed metal ions [72]. In these cases, dissolving the deposits would obviously prevent their own toxicity, and the net outcome would depend on the balance between the toxic and protective influences of the deposits in a particular patient.

LIST OF ABBREVIATIONS

AD	=	Alzheimer's Disease
NC	=	Normal Cognition
Aβ	=	Beta-amyloid
Aβ42	=	$A\beta_{1\text{-}42}$
CSF	=	Cerebrospinal Fluid
CSF-Aβ42	=	Concentration of Aβ42 in the CSF
PET	=	Positron Emission Tomography

ETHICS APPROVAL AND CONSENT TO PARTICIPATE

The study protocol for ADNI was approved by the all participating institutions.

HUMAN AND ANIMAL RIGHTS

All human procedures were followed in accordance with the guidelines of Helsinki.

CONSENT FOR PUBLICATION

All participant signed informed consent.

AVAILABILITY OF DATA AND MATERIALS

The data and supportive information are available within the article.

FUNDING

Data collection and sharing for this project was funded by the Alzheimer's Disease Neuroimaging Initiative (ADNI) (NIH Grant U01 AG024904) and DOD ADNI (award number W81XWH-12-2-0012). ADNI is funded by the National Institute on Aging, the National Institute of Biomedical Imaging and Bioengineering, and through generous contributions from the following: AbbVie; Alzheimer's Association; Alzheimer's Drug Discovery Foundation; Araclon Biotech; BioClinica, Inc.; Biogen; Bristol-Myers Squibb Company; CereSpir, Inc.; Cogstate; Eisai Inc.; Elan Pharmaceuticals, Inc.; Eli Lilly and Company; EuroImmun; F. Hoffmann-La Roche Ltd and its affiliated company Genentech, Inc.; Fujirebio; GE Healthcare; IXICO Ltd.; Janssen Alzheimer Immunotherapy Research & Development, LLC.; Johnson & Johnson Pharmaceutical Research & Development LLC.; Lumosity; Lundbeck; Merck & Co., Inc.; Meso Scale Diagnostics, LLC.; NeuroRx Research; Neurotrack Technologies; Novartis Pharmaceuticals Corporation; Pfizer Inc.; Piramal

Imaging; Servier; Takeda Pharmaceutical Company; and Transition Therapeutics. The Canadian Institutes of Health Research is providing funds to support ADNI clinical sites in Canada. Private sector contributions are facilitated by the Foundation for the National Institutes of Health (www.fnih.org). The grantee organization is the Northern California Institute for Research and Education, and the study is coordinated by the Alzheimer's Therapeutic Research Institute at the University of Southern California. ADNI data are disseminated by the Laboratory for Neuro Imaging at the University of Southern California.

CONFLICT OF INTEREST

The authors declare no conflict of interest, financial or otherwise.

ACKNOWLEDGEMENTS

The authors thank Daniel Zaretsky for his editorial help.

SUPPLEMENTARY MATERIAL

Supplementary material is available on the publisher's website along with the published article.

REFERENCES

[1] Alzheimer A. About peculiar illnesses of later age. Z Gesamte Neurol Psychiatr 1911; 4(1): 356-85. http://dx.doi.org/10.1007/BF02866241

[2] Graeber MB, Mehraein P. Reanalysis of the first case of Alzheimer's disease. Eur Arch Psychiatry Clin Neurosci 1999; 249(S3): S10-3. http://dx.doi.org/10.1007/PL00014167 PMID: 10654094

[3] Glenner GG. Amyloid beta protein and the basis for Alzheimer's disease. Prog Clin Biol Res 1989; 317: 857-68. PMID: 2690126

[4] Glenner GG, Wong CW. Alzheimer's disease: Initial report of the purification and characterization of a novel cerebrovascular amyloid protein. Biochem Biophys Res Commun 1984; 120(3): 885-90. http://dx.doi.org/10.1016/S0006-291X(84)80190-4 PMID: 6375662

[5] Demuro A, Mina E, Kayed R, Milton SC, Parker I, Glabe CG. Calcium dysregulation and membrane disruption as a ubiquitous neurotoxic mechanism of soluble amyloid oligomers. J Biol Chem 2005; 280(17): 17294-300. http://dx.doi.org/10.1074/jbc.M500997200 PMID: 15722360

[6] Cline EN, Bicca MA, Viola KL, Klein WL. The amyloid-β oligomer hypothesis: Beginning of the third decade. J Alzheimers Dis 2018; 64(s1): S567-610. http://dx.doi.org/10.3233/JAD-179941 PMID: 29843241

[7] Lambert MP, Barlow AK, Chromy BA, *et al.* Diffusible, nonfibrillar ligands derived from Abeta1-42 are potent central nervous system neurotoxins. Proc Natl Acad Sci 1998; 95(11): 6448-53. http://dx.doi.org/10.1073/pnas.95.11.6448

[8] Knafo S, Alonso-Nanclares L, Gonzalez-Soriano J, *et al.* Widespread changes in dendritic spines in a model of Alzheimer's disease. Cereb Cortex 2009; 19(3): 586-92. http://dx.doi.org/10.1093/cercor/bhn111

[9] Tsai J, Grutzendler J, Duff K, Gan WB. Fibrillar amyloid deposition leads to local synaptic abnormalities and breakage of neuronal branches. Nat Neurosci 2004; 7(11): 1181-3. http://dx.doi.org/10.1038/nn1335 PMID: 15475950

[10] Bittner T, Fuhrmann M, Burgold S, *et al.* Multiple events lead to dendritic spine loss in triple transgenic Alzheimer's disease mice. PLoS One 2010; 5(11): e15477. http://dx.doi.org/10.1371/journal.pone.0015477 PMID: 21103384

[11] Mattsson N, Insel PS, Landau S, *et al.* Diagnostic accuracy of CSF Ab42 and florbetapir PET for Alzheimer's disease. Ann Clin Transl Neurol 2014; 1(8): 534-43. http://dx.doi.org/10.1002/acn3.81

[12] Ong KT, Villemagne VL, Bahar-Fuchs A, *et al.* Aβ imaging with 18F-florbetaben in prodromal Alzheimer's disease: A prospective outcome study. J Neurol Neurosurg Psychiatry 2015; 86(4): 431-6. http://dx.doi.org/10.1136/jnnp-2014-308094 PMID: 24970906

[13] Weigand SD, Vemuri P, Wiste HJ, *et al.* Transforming cerebrospinal fluid Aβ42 measures into calculated Pittsburgh Compound B units of brain Aβ amyloid. Alzheimers Dement 2011; 7(2): 133-41. http://dx.doi.org/10.1016/j.jalz.2010.08.230

[14] Mattsson N, Insel PS, Donohue M, *et al.* Independent information from cerebrospinal fluid amyloid-β and florbetapir imaging in Alzheimer's disease. Brain 2015; 138(Pt 3): 772-83. http://dx.doi.org/10.1093/brain/awu367

[15] Fagan AM, Mintun MA, Mach RH, *et al.* Inverse relation between *in vivo* amyloid imaging load and cerebrospinal fluid $A\beta_{42}$ in humans. Ann Neurol 2006; 59(3): 512-9. http://dx.doi.org/10.1002/ana.20730 PMID: 16372280

[16] Sturchio A, Dwivedi AK, Young CB, *et al.* High cerebrospinal amyloid-β 42 is associated with normal cognition in individuals with brain amyloidosis. EClinicalMedicine 2021; 38: 100988. http://dx.doi.org/10.1016/j.eclinm.2021.100988 PMID: 34505023

[17] Mawuenyega KG, Sigurdson W, Ovod V, *et al.* Decreased clearance of CNS beta-amyloid in Alzheimer's disease. Science 2010; 330(6012): 1774. http://dx.doi.org/10.1126/science.1197623

[18] Silverberg GD, Heit G, Huhn S, *et al.* The cerebrospinal fluid production rate is reduced in dementia of the Alzheimer's type. Neurology 2001; 57(10): 1763-6. http://dx.doi.org/10.1212/WNL.57.10.1763 PMID: 11723260

[19] Fishman RA. The cerebrospinal fluid production rate is reduced in dementia of the Alzheimer's type. Neurology 2002; 58(12): 1866. http://dx.doi.org/10.1212/WNL.58.12.1866

[20] Zaretsky DV, Zaretskaia MV, Molkov YI. Patients with Alzheimer's disease have an increased removal rate of soluble beta-amyloid-42. PLoS One 2022; 17(10): e0276933. http://dx.doi.org/10.1371/journal.pone.0276933 PMID: 36315527

[21] Zaretsky DV, Zaretskaia MV. Mini-review: Amyloid degradation toxicity hypothesis of Alzheimer's disease. Neurosci Lett 2021; 756: 135959. http://dx.doi.org/10.1016/j.neulet.2021.135959 PMID: 34000347

[22] Zaretsky DV, Zaretskaia M. Degradation products of amyloid protein: Are they the culprits? Curr Alzheimer Res 2021; 17(10): 869-80. http://dx.doi.org/10.2174/1567205017666201203142103 PMID: 33272185

[23] Zaretsky DV, Zaretskaia MV. Flow cytometry method to quantify the formation of beta-amyloid membrane ion channels. Biochim Biophys Acta Biomembr 2020; 1863(2): 183506. http://dx.doi.org/10.1016/j.bbamem.2020.183506 PMID: 33171157

[24] Yang AJ, Chandswangbhuvana D, Margol L, Glabe CG. Loss of endosomal/lysosomal membrane impermeability is an early event in amyloid A?1-42 pathogenesis. J Neurosci Res 1998; 52(6): 691-8. http://dx.doi.org/10.1002/(SICI)1097-4547(19980615)52:6<691::AID-JNR8>3.0.CO;2-3 PMID: 9669318

[25] Ji ZS, Miranda RD, Newhouse YM, Weisgraber KH, Huang Y, Mahley RW. Apolipoprotein E4 potentiates amyloid beta peptide-induced lysosomal leakage and apoptosis in neuronal cells. J Biol Chem 2002; 277(24): 21821-8. http://dx.doi.org/10.1074/jbc.M112109200 PMID: 11912196

[26] Arispe N, Pollard HB, Rojas E. Giant multilevel cation channels formed by Alzheimer disease amyloid beta-protein [A beta P-(1-40)] in bilayer membranes. Proc Natl Acad Sci 1993; 90(22): 10573-7. http://dx.doi.org/10.1073/pnas.90.22.10573 PMID: 7504270

[27] Lin MA, Kagan BL. Electrophysiologic properties of channels induced by Aβ25–35 in planar lipid bilayers. Peptides 2002; 23(7): 1215-28. http://dx.doi.org/10.1016/S0196-9781(02)00057-8 PMID: 12128079

[28] Mirzabekov T, Lin MC, Yuan WL, *et al.* Channel formation in planar lipid bilayers by a neurotoxic fragment of the beta-amyloid peptide. Biochem Biophys Res Commun 1994; 202(2): 1142-8. http://dx.doi.org/10.1006/bbrc.1994.2047 PMID: 7519420

[29] Zaretsky DV, Zaretskaia MV, Molkov YI. Membrane channel hypothesis of lysosomal permeabilization by beta-amyloid. Neurosci Lett 2021; 770: 136338. http://dx.doi.org/10.1016/j.neulet.2021.136338 PMID: 34767924

[30] Guicciardi ME, Leist M, Gores GJ. Lysosomes in cell death. Oncogene 2004; 23(16): 2881-90. http://dx.doi.org/10.1038/sj.onc.1207512 PMID: 15077151

[31] Kavčič N, Pegan K, Turk B. Lysosomes in programmed cell death pathways: From initiators to amplifiers. Biol Chem 2017; 398(3): 289-301. http://dx.doi.org/10.1515/hsz-2016-0252 PMID: 28002019

[32] Turk B, Stoka V, Rozman-Pungercar J, *et al.* Apoptotic pathways: Involvement of lysosomal proteases. Biol Chem 2002; 383(7-8): 1035-44. http://dx.doi.org/10.1515/BC.2002.112 PMID: 12437086

[33] Jakoš T, Pišlar A, Jewett A, Kos J. Cysteine cathepsins in tumor-associated immune cells. Front Immunol 2019; 10(2037): 2037. http://dx.doi.org/10.3389/fimmu.2019.02037 PMID: 31555270

[34] Alzheimer's Disease Neuroimaging Initiative (ADNI) Data Sharing and Publication Policy. 2016. Available from: https://adni.loni.usc.edu/wp-content/uploads/how_to_apply/ADNI_DSP_Policy.pdf

[35] 2020 Alzheimer's disease facts and figures. Alzheimers Dement 2020; 16(3): 391-460. http://dx.doi.org/10.1002/alz.12068

[36] Fagan AM. What does it mean to be 'amyloid-positive'? Brain 2015; 138(3): 514-6. http://dx.doi.org/10.1093/brain/awu387 PMID: 25713403

[37] Andreasen N, Hesse C, Davidsson P, *et al.* Cerebrospinal fluid β-amyloid(1-42) in Alzheimer disease: Differences between early- and late-onset Alzheimer disease and stability during the course of disease. Arch Neurol 1999; 56(6): 673-80. http://dx.doi.org/10.1001/archneur.56.6.673 PMID: 10369305

[38] Schubert D. Serpins inhibit the toxicity of amyloid peptides. Eur J Neurosci 1997; 9(4): 770-7. http://dx.doi.org/10.1111/j.1460-9568.1997.tb01425.x PMID: 9153583

[39] Budd Haeberlein SL, Aisen PS, Barkhof F, *et al.* Two randomized phase 3 studies of aducanumab in early alzheimer's disease. J Prev Alzheimers Dis 2022; 9(2): 197-210. http://dx.doi.org/10.14283/jpad.2022.30 PMID: 35542991

[40] Egan MF, Kost J, Tariot PN, *et al.* Randomized trial of verubecestat for mild-to-moderate Alzheimer's Disease. N Engl J Med 2018; 378(18): 1691-703. http://dx.doi.org/10.1056/NEJMoa1706441 PMID: 29719179

[41] Wessels AM, Lines C, Stern RA, *et al.* Cognitive outcomes in trials of two BACE inhibitors in Alzheimer's disease. Alzheimers Dement 2020; 16(11): 1483-92. http://dx.doi.org/10.1002/alz.12164 PMID: 33049114

[42] Mueller SG, Weiner MW, Thal LJ, *et al.* The Alzheimer's disease neuroimaging initiative. Neuroimaging Clin N Am 2005; 15(4): 869-77. http://dx.doi.org/10.1016/j.nic.2005.09.008

[43] Mueller SG, Weiner MW, Thal LJ, *et al.* Ways toward an early diagnosis in Alzheimer's disease: The Alzheimer's Disease Neuroimaging Initiative (ADNI). Alzheimers Dement 2005; 1(1): 55-66. http://dx.doi.org/10.1016/j.jalz.2005.06.003

[44] Arispe N, Pollard HB, Rojas E. β-amyloid Ca^{2+}-channel hypothesis for neuronal death in Alzheimer Disease. Mol Cell Biochem 1994; 140(2): 119-25. http://dx.doi.org/10.1007/BF00926750 PMID: 7898484

[45] Arispe N, Rojas E, Pollard HB. Alzheimer disease amyloid beta protein forms calcium channels in bilayer membranes: Blockade by tromethamine and aluminum. Proc Natl Acad Sci 1993; 90(2): 567-71. http://dx.doi.org/10.1073/pnas.90.2.567 PMID: 8380642

[46] Pollard HB, Rojas E, Arispe N. A new hypothesis for the mechanism of amyloid toxicity, based on the calcium channel activity of amyloid beta protein (A beta P) in phospholipid bilayer membranes. Ann N Y Acad Sci 1993; 695(1): 165-8. http://dx.doi.org/10.1111/j.1749-6632.1993.tb23046.x PMID: 8239277

[47] Millucci L, Ghezzi L, Bernardini G, Santucci A. Conformations and biological activities of amyloid beta peptide 25-35. Curr Protein Pept Sci 2010; 11(1): 54-67. http://dx.doi.org/10.2174/138920310790274626 PMID: 20201807

[48] Karkisaval AG, Rostagno A, Azimov R, *et al.* Ion channel formation by N-terminally truncated Aβ (4–42): Relevance for the pathogenesis of Alzheimer's disease. Nanomedicine 2020; 29: 102235. http://dx.doi.org/10.1016/j.nano.2020.102235 PMID: 32531337

[49] Jang H, Arce FT, Ramachandran S, *et al.* Truncated β-amyloid peptide channels provide an alternative mechanism for Alzheimer's Disease and Down syndrome. Proc Natl Acad Sci 2010; 107(14): 6538-43. http://dx.doi.org/10.1073/pnas.0914251107 PMID: 20308552

[50] Hirakura Y, Lin MC, Kagan BL. Alzheimer amyloid aβ1-42 channels: Effects of solvent, pH, and congo red. J Neurosci Res 1999; 57(4): 458-66. http://dx.doi.org/10.1002/(SICI)1097-4547(19990815)57:4<458::AID-JNR5>3.0.CO;2-4 PMID: 10440895

[51] Bevers EM, Williamson PL. Getting to the outer leaflet: Physiology of phosphatidylserine exposure at the plasma membrane. Physiol Rev 2016; 96(2): 605-45. http://dx.doi.org/10.1152/physrev.00020.2015 PMID: 26936867

[52] Wesén E, Jeffries GDM, Matson Dzebo M, Esbjörner EK. Endocytic uptake of monomeric amyloid-β peptides is clathrin- and dynamin-independent and results in selective accumulation of Aβ(1-42) compared to Aβ(1-40). Sci Rep 2021; 7(1): 2021. http://dx.doi.org/10.1038/s41598-017-02227-9

[53] Colacurcio DJ, Pensalfini A, Jiang Y, Nixon RA. Dysfunction of autophagy and endosomal-lysosomal pathways: Roles in pathogenesis of Down syndrome and Alzheimer's Disease. Free Radic Biol Med 2018; 114: 40-51. http://dx.doi.org/10.1016/j.freeradbiomed.2017.10.001

[54] Nixon RA, Wegiel J, Kumar A, *et al.* Extensive involvement of autophagy in Alzheimer disease: An immuno-electron microscopy study. J Neuropathol Exp Neurol 2005; 64(2): 113-22. http://dx.doi.org/10.1093/jnen/64.2.113 PMID: 15751225

[55] Rhein V, Baysang G, Rao S, *et al.* Amyloid-beta leads to impaired cellular respiration, energy production and mitochondrial electron chain complex activities in human neuroblastoma cells. Cell Mol Neurobiol 2009; 29(6-7): 1063-71. http://dx.doi.org/10.1007/s10571-009-9398-y PMID: 19350381

[56] Schmitt K, Grimm A, Kazmierczak A, Strosznajder JB, Götz J, Eckert A. Insights into mitochondrial dysfunction: Aging, amyloid-β, and tau-A deleterious trio. Antioxid Redox Signal 2012; 16(12): 1456-66. http://dx.doi.org/10.1089/ars.2011.4400 PMID: 22117646

[57] Eckert A, Schmitt K, Götz J. Mitochondrial dysfunction - the beginning of the end in Alzheimer's disease? Separate and synergistic modes of tau and amyloid-β toxicity. Alzheimers Res Ther 2011; 3(2): 15. http://dx.doi.org/10.1186/alzrt74

[58] Gupta A. Role of caspases, apoptosis and additional factors in pathology of Alzheimer's disease. In: *Gupta A, Ed. Human Caspases and Neuronal Apoptosis in Neurodegenerative Diseases.* Academic Press, Cambridge, Massachusetts, 2022; pp. 69-151. http://dx.doi.org/10.1016/B978-0-12-820122-0.00001-7

[59] Haass C, Kaether C, Thinakaran G, Sisodia S. Trafficking and proteolytic processing of APP. Cold Spring Harb Perspect Med 2012; 2(5): a006270. http://dx.doi.org/10.1101/cshperspect.a006270

[60] Selkoe DJ, Hardy J. The amyloid hypothesis of Alzheimer's disease at 25 years. EMBO Mol Med 2016; 8(6): 595-608. http://dx.doi.org/10.15252/emmm.201606210

[61] Murphy MP, LeVine H 3rd. Alzheimer's disease and the amyloid-beta peptide. J Alzheimers Dis 2010; 19(1): 311-23. http://dx.doi.org/10.3233/JAD-2010-1221

[62] Im D, Heo CE, Son MK, Park CR, Kim HI, Choi JM. Kinetic modulation of amyloid-β (1–42) aggregation and toxicity by structure-based rational design. J Am Chem Soc 2022; 144(4): 1603-11.

http://dx.doi.org/10.1021/jacs.1c10173 PMID: 35073692

[63] Cohen SIA, Linse S, Luheshi LM, *et al.* Proliferation of amyloid-β42 aggregates occurs through a secondary nucleation mechanism. Proc Natl Acad Sci 2013; 110(24): 9758-63. http://dx.doi.org/10.1073/pnas.1218402110

[64] Patterson BW, Elbert DL, Mawuenyega KG, *et al.* Age and amyloid effects on human central nervous system amyloid-beta kinetics. Ann Neurol 2015; 78(3): 439-53. http://dx.doi.org/10.1002/ana.24454

[65] Hu X, Crick SL, Bu G, Frieden C, Pappu RV, Lee JM. Amyloid seeds formed by cellular uptake, concentration, and aggregation of the amyloid-beta peptide. Proc Natl Acad Sci 2009; 106(48): 20324-9. http://dx.doi.org/10.1073/pnas.0911281106 PMID: 19910533

[66] Burdick D, Kosmoski J, Knauer MF, Glabe CG. Preferential adsorption, internalization and resistance to degradation of the major isoform of the Alzheimer's amyloid peptide, Aβ1–42, in differentiated PC12 cells. Brain Res 1997; 746(1-2): 275-84. http://dx.doi.org/10.1016/S0006-8993(96)01262-0 PMID: 9037507

[67] Bonam SR, Wang F, Muller S. Lysosomes as a therapeutic target. Nat Rev Drug Discov 2019; 18(12): 923-48. http://dx.doi.org/10.1038/s41573-019-0036-1 PMID: 31477883

[68] Mathews PM, Levy E. Cystatin C in aging and in Alzheimer's disease. Ageing Res Rev 2016; 32: 38-50. http://dx.doi.org/10.1016/j.arr.2016.06.003 PMID: 27333827

[69] Bischof GN, Rodrigue KM, Kennedy KM, Devous MD Sr, Park DC. Amyloid deposition in younger adults is linked to episodic memory performance. Neurology 2016; 87(24): 2562-6. http://dx.doi.org/10.1212/WNL.0000000000003425

[70] Potter R, Patterson BW, Elbert DL, *et al.* Increased *in vivo* amyloid-β42 production, exchange, and loss in presenilin mutation carriers. Sci Transl Med 2013; 5(189): 189ra77. http://dx.doi.org/10.1126/scitranslmed.3005615

[71] Wallin H, Bjarnadottir M, Vogel LK, Wassélius J, Ekström U, Abrahamson M. Cystatins- extra- and intracellular cysteine protease inhibitors: High-level secretion and uptake of cystatin C in human neuroblastoma cells. Biochimie 2010; 92(11): 1625-34. http://dx.doi.org/10.1016/j.biochi.2010.08.011 PMID: 20800088

[72] Wang T, Xu SF, Fan YG, Li LB, Guo C. Iron pathophysiology in Alzheimer's Diseases. Adv Exp Med Biol 2019; 1173: 67-104. http://dx.doi.org/10.1007/978-981-13-9589-5_5 PMID: 31456206